

**Network view of SST
variability**

A. Tantet and
H. A. Dijkstra

This discussion paper is/has been under review for the journal Earth System Dynamics (ESD). Please refer to the corresponding final paper in ESD if available.

An interaction network perspective on the relation between patterns of sea surface temperature variability and global mean surface temperature

A. Tantet and H. A. Dijkstra

Institute for Marine and Atmospheric research Utrecht, Utrecht University,
Utrecht, the Netherlands

Received: 25 July 2013 – Accepted: 1 August 2013 – Published: 12 August 2013

Correspondence to: A. Tantet (a.j.j.tantet@uu.nl)

Published by Copernicus Publications on behalf of the European Geosciences Union.

Title Page

Abstract

Introduction

Conclusions

References

Tables

Figures

◀

▶

◀

▶

Back

Close

Full Screen / Esc

Printer-friendly Version

Interactive Discussion



Abstract

On interannual-to-multidecadal time scales variability in sea surface temperature appears to be organized in large-scale spatiotemporal patterns. In this paper, we investigate these patterns by studying the community structure of interaction networks constructed from sea surface temperature observations. Much of the community structure as well as the first neighbour maps can be interpreted using known dominant patterns of variability, such as the El Niño/Southern Oscillation and the Atlantic Multidecadal Oscillation and teleconnections. The community detection method allows to overcome some shortcomings of Empirical Orthogonal Function analysis or composite analysis and hence provides additional information with respect to these classical analysis tools. The community analysis provides also new insight into the relationship between patterns of sea surface temperature and the global mean surface temperature (GMST). On the decadal-to-multidecadal time scale, we show that only two communities (Indian Ocean and North Atlantic) determine most of the GMST variability.

1 Introduction

An important issue in climate research is to understand the behavior of the global mean surface temperature (GMST) over the last century (Sutton et al., 2007). Both internal variability and changes in radiative forcing, in particular by anthropogenic emissions of greenhouse gases (GHG), contribute to changes in GMST. The impact of GHG forcing has been extensively studied, being highly relevant to climate sensitivity and hence for projections on future changes of the GMST. The important role of internal variability of ocean heat storage on GMST has been highlighted in the recent study by Balmaseda et al. (2013).

On interannual-to-multidecadal time scales, climate variability appears to be organized into large-scale patterns with the El Niño/Southern Oscillation (ENSO) and the Atlantic Multidecadal Oscillation (AMO) as prominent examples. These phenomena

ESDD

4, 743–783, 2013

Network view of SST variability

A. Tantet and
H. A. Dijkstra

Title Page

Abstract

Introduction

Conclusions

References

Tables

Figures

◀

▶

◀

▶

Back

Close

Full Screen / Esc

Printer-friendly Version

Interactive Discussion



Network view of SST variability

A. Tantet and
H. A. Dijkstra

Title Page

Abstract

Introduction

Conclusions

References

Tables

Figures



Back

Close

Full Screen / Esc

Printer-friendly Version

Interactive Discussion



are characterized by well defined spatiotemporal patterns in sea surface temperature (SST). The ENSO variability in the equatorial Pacific is the dominant pattern of variability on interannual time-scales (McPhaden et al., 1998; Wang et al., 2004). The AMO is the dominant pattern of SST variability in the North Atlantic on decadal-to-multidecadal time scales Enfield (2001). ENSO influences the climate of many regions over the globe (Alexander and Bladé, 2002; Deser et al., 2010) and the El Niño 1997–1998 event was estimated to have caused a GMST increase of about 0.6°C Trenberth (1997). Sutton and Hodson (2005) show that the AMO has an influence on European summer temperatures and relations of the AMO with US rainfall were suggested in Enfield (2001). Recently, it was suggested that the variability of global land surface temperatures (GLST) is strongly connected to the AMO Muller et al. (2013), with a correlation coefficient of 0.65 ± 0.04 .

In most studies so far on the connection between patterns of variability and GMST, variants of empirical orthogonal function analysis (EOF, von Storch and Zwiers, 1999a) have been used to identify spatial patterns of variability. The disadvantage of EOF's, when computed from the global SST field, is that only the dominant mode can be clearly associated to a spatiotemporal pattern of variability. Higher order modes, which are required to be orthogonal to the first mode, are usually difficult to relate to the patterns of variability as known from regional EOF analyses Monahan et al. (2009). It is therefore still quite unclear how and how much the different patterns and their interaction contribute to GMST variability.

Here we address the problem on the connection between patterns of SST variability and GMST using complex networks theory. Although this theory has already been successfully applied to many different technological and scientific problems (e.g. in computer sciences, neurosciences, social sciences) it is only recent that it is used in climate research. So-called interaction networks, where links are based on a correlation measure between variables at specific locations, have been reconstructed to analyze the connectivity of the climate system (Tsonis and Roebber, 2004; Tsonis et al., 2010; Donges et al., 2009a, b), teleconnections (Tsonis et al., 2008), the behavior of El Niño

(Gozolchiani et al., 2008, 2011; Tsonis and Swanson, 2008; Yamasaki et al., 2008), synchronization between different spatiotemporal patterns (Tsonis et al., 2007; Wyatt et al., 2011) and the connections between the variability in different climate variables (Donges et al., 2011).

5 One of the many interesting properties of a network is its possible partition into communities or groups of highly connected nodes which are only weakly connected to the rest of the network. Community detection has recently been applied to climate interaction networks of different atmospheric variables from observations and simulations by Tsonis et al. (2010) where some of the known patterns of atmospheric variability, such as North Atlantic Oscillation, could be identified.

10 We focus in this study on communities in interaction networks reconstructed from global SST observations. The data, their preprocessing and the network reconstruction and analysis tools are presented in Sect. 2. In Sect. 3, results on the SST communities in the reconstructed networks are presented and interpreted, and connected to results in the literature based on EOF and composite analysis. Then in Sect. 4, we address the connection between the SST communities and the GMST and compare the results from observations with those from Earth System Model (ESM) simulations. In the last Sect. 5, the main results are summarized and discussed with a focus on the benefits of the interaction network approach.

20 **2 Data and methods**

2.1 Data and network reconstruction

Monthly mean SST observations over the period 1870 to 2011 compiled in the HadISST dataset (Rayner, 2003) were used. The seasonal cycle was removed from the linearly detrended monthly data. Even though the leading order effect of the annual cycle is removed by producing anomaly values, boreal winter anomalies are still larger than in summer. In order to avoid spurious high values of correlations, Tsonis and

Network view of SST variability

A. Tantet and
H. A. Dijkstra

Title Page

Abstract

Introduction

Conclusions

References

Tables

Figures



Back

Close

Full Screen / Esc

Printer-friendly Version

Interactive Discussion



Network view of SST variability

A. Tantet and
H. A. Dijkstra

Title Page

Abstract

Introduction

Conclusions

References

Tables

Figures

◀

▶

◀

▶

Back

Close

Full Screen / Esc

Printer-friendly Version

Interactive Discussion



Roebber (2004) and Tsonis et al. (2010) only used the December-January-February months of each year. Since our results were not significantly affected by the selection of the winter months, we decided to use complete years. The detrended monthly anomalies were then filtered via a Lanczos filter (Duchon, 1979) with a cutoff frequency of $1/13 \text{ month}^{-1}$ and order 144.

Because there are more grid points towards the poles on a regular longitude-latitude grid, which could lead to biases in our network measures, the data were linearly interpolated on an unstructured grid conserving the arc length with latitude. In this study, we used a resolution at the equator of 2° but the results presented bellow are qualitatively identical when using grid resolutions ranging from 1 to 5° . Because of the poor sampling of the region south of 50°S , only the grid-points between 50°S and 80°N were kept, resulting in a total of $N = 6280$ grid points (land surface points excluded) for $L = 142 \times 12 = 1704$ months.

Each ocean grid point is considered as a node in the network and we indicate the time series at node i , $i = 1, \dots, N$ by $p_i(t_k)$, $k = 1, \dots, L$. Contrary to a network as derived from a power grid or the world-wide web, the links of a climate network are not directly tangible because the observables derive from continuous fields. In an interaction network, a link between two nodes is based on a measure of the correlation between the time series of these two nodes. In this study, we used the Pearson correlation coefficient at lag zero, say R_{ij} , between the time series of nodes i and j , defined by

$$R_{ij} = \frac{\sum_{k=1}^L p_i(t_k) p_j(t_k)}{\sqrt{(\sum_{k=1}^L p_i^2(t_k)) (\sum_{k=1}^L p_j^2(t_k))}}. \quad (1)$$

as the measure defining the links in the network Tsonis and Roebber (2004). A pair of nodes is then considered to be connected if their correlation R_{ij} is over a chosen threshold τ . The elements a_{ij} of the $N \times N$ adjacency matrix \mathbf{A} of the undirected and unweighted network are thus given by:

$$a_{ij} = \Theta(R_{ij} - \tau) - \delta_{ij} \quad (2)$$

where Θ and δ are the Heaviside function and Kronecker symbol, respectively. Even though the links in the network are based on SST correlations at zero lag, a connection is not only representative of instantaneous relationship, since the time series are 13 months low-pass filtered.

We based our choice of the threshold τ on parametric and non-parametric significance tests. Considering a decorrelation time of 13 months (corresponding to the cut-off frequency of the filter), we found that all correlations over 0.17 are statistically significant at the 95 % level according to a t test with $L/13 = 131^\circ$ of freedom.

In order to better account for the persistence in the time series, a moving block bootstrap (MBB) test was also applied to the time series Mudelsee (2010). The bootstrap works with artificially produced resamples of the time series. In an MBB, blocks of length L_B are randomly picked out of the original time series to create a set of size N_S of surrogate time series. Correlations are then calculated between surrogate time series for each pair of nodes. The choice of the block-length is a trade-off between conserving the memory of the original time series and producing maximally independent surrogate time series. For the dataset used in this study, we found that the estimated 95 % significance level was robust for block lengths ranging from 15 to 50 yr. Consequently, we chose a block length of L_B of 20 yr and a sample set size N_S of 4000 for all our MBB tests. Because a grid of 6280 nodes results in $\sim 2 \times 10^7$ pairs, the MBB tests were realized on a coarser grid of $5^\circ \times 5^\circ$ resulting in 1144 nodes. We found that in the worst case the p -value of the 95 % significance level was 0.39.

Additionally, an approximate test was used, where correlations were calculated between pairs of surrogate time series associated with the same node for the 6280 nodes of the 2° grid. The p values found in this case were close to the maximum p values found for each grid point of the first test, suggesting that the approximated version of the MBB test is a good alternative for large gridded datasets.

Network view of SST variability

A. Tantet and
H. A. Dijkstra

Title Page	
Abstract	Introduction
Conclusions	References
Tables	Figures
◀	▶
◀	▶
Back	Close
Full Screen / Esc	
Printer-friendly Version	
Interactive Discussion	



Network view of SST variability

A. Tantet and
H. A. Dijkstra

Title Page

Abstract

Introduction

Conclusions

References

Tables

Figures

◀

▶

◀

▶

Back

Close

Full Screen / Esc

Printer-friendly Version

Interactive Discussion



The results of both parametric and non-parametric tests indicate that a threshold $\tau = 0.4$ guarantees that a link between a pair of nodes of the HadISST data represents a statistically significant correlation at the 95 % level. In addition, thresholds ranging from 0.4 to 0.6 were used to build the network and we found that our results were not qualitatively sensitive to the threshold value over this range, although teleconnections appear weaker as the threshold increases. Subsequently, a threshold of 0.4 will be used and the resulting interaction network build from the HadISST dataset will be referred to as the H-SST network.

2.2 Analysis techniques

Extended reviews of commonly used network measures can be found in Costa and Rodrigues (2007) and Barthélemy (2011). We here focus on degree centrality, first-neighbour maps and communities. The degree centrality d_i of a node i counts its number of connections with other nodes of the network. This measure is directly accessible from the adjacency matrix through

$$d_i = \sum_{j=1}^N a_{ij} \quad (3)$$

and allows to reveal nodes sharing a common variability with other nodes of the network. The edge density ρ of a network

$$\rho = \frac{1}{N(N-1)} \sum_{i,j=1}^N a_{ij} \quad (4)$$

is the total number of links in the network normalized by the maximum number of possible links and is an indicator of the sparseness of the network. First-neighbours map provide insight into the connections of all nodes in the network to a selected group of nodes. A node of a first-neighbour map reaches a maximum (minimum) value

of 100% (0%) if it is connected to all (none) of the nodes of the selected group of nodes.

Much focus has recently been given to the partitioning of networks into communities (Newman and Girvan, 2004). Communities are groups of nodes tightly connected together and weakly connected to the rest of the network. As such, they can be regarded as subsystems which operate relatively independently of the other communities (Arenas et al., 2006). Considerable improvements have been made during the past decade regarding the speed and efficiency of the community detection algorithms. In Tsonis et al. (2010), the algorithm of Newman and Girvan (2004) based on the progressive removal of dominant links (in terms of information flow) was applied to determine the community structure of several fields (500 hPa height, sea level pressure and surface temperature) derived from the NCEP/NCAR reanalysis (Kistler et al., 2001) and simulations from the GFDL CM2.1 model (Delworth, 2006).

We tested the Multilevel algorithm of Blondel et al. (2008) and the Leading Eigenvector algorithm of Newman (2006) which, as the algorithm used by Tsonis et al. (2010), is based on the optimization of the modularity (cf. Sect. 3.1) but has a faster implementation. However, results presented in Sect. 3 below are generated using the Infomap algorithm by Rosvall and Bergstrom (2007) which is based on the compression of the paths of random walkers traveling along the network. This algorithm was the most efficient in the LFR benchmark Lancichinetti and Fortunato (2009) among the different algorithms tested.

3 Spatial structure of SST variability

3.1 Communities in the H-SST network: detection

The map of degree centrality of the H-SST networks (Fig. 1) indicates that nodes in the tropics tend to have a higher degree centrality than those in the extra-tropics, in agreement with atmospheric surface temperature analyses in Tsonis and Roebber (2004).

Network view of SST variability

A. Tantet and
H. A. Dijkstra

Title Page

Abstract

Introduction

Conclusions

References

Tables

Figures



Back

Close

Full Screen / Esc

Printer-friendly Version

Interactive Discussion



Network view of SST variability

A. Tantet and
H. A. Dijkstra

Title Page

Abstract

Introduction

Conclusions

References

Tables

Figures

◀

▶

◀

▶

Back

Close

Full Screen / Esc

Printer-friendly Version

Interactive Discussion



The tropical Atlantic shows a rather low degree centrality compared to the Indian and Pacific Oceans except over its northwestern part. The eastern tropical Indian Ocean also shows a low degree centrality. Surrounding the tropics, patches of high degree centrality are found in the midlatitude North Pacific, South Pacific and along the western coast of the American continent.

In order to assess whether the variability in high degree regions arises from distinct spatial patterns, the community structure of the H-SST network is determined (Fig. 2a). The communities are ordered by the total PageRank of their nodes (Brin and Page, 1998), which corresponds to the steady state flow of random walkers through the nodes of the community. The larger the PageRank of a community the higher the probability of random walkers to travel through the community.

A common measure of the quality of a partition of a network into communities is the modularity of this partition (Newman and Girvan, 2004). For a particular division into m communities an $m \times m$ symmetric matrix \mathbf{e} is defined, for which an element e_{ij} is the fraction of all connections in the network that link nodes in community i to nodes in community j . As such, $\sum_i e_{ij}$ gives the fraction of edges in the network that connect nodes in the same community and $f_i = \sum_j e_{ij}$ represents the fraction of all edges in the network that connect to nodes in community i . In a (random) network, for which edges connect nodes independent of the communities they belong to, we would have $e_{ij} = f_i f_j$ so that $\sum_i f_i^2$ corresponds to the fraction of all edges that connect to the same community in such a randomly wired network. In a modular network, the (e_{ij}) must be high comparatively to the (f_i^2) . Thus, the modularity M is defined as (Newman and Girvan, 2004)

$$M = \sum_{i=1}^m \left(e_{ii} - f_i^2 \right). \quad (5)$$

The modularity of the Infomap partition of the H-SST network into 11 communities (Fig. 2a) is $M = 0.23$, which is smaller than the modularities of 0.29 and 0.28 of the partitions into 5 and 7 communities of the Multilevel and Leading Eigenvector algo-

Network view of SST variability

A. Tantet and
H. A. Dijkstra

Title Page

Abstract

Introduction

Conclusions

References

Tables

Figures

⏪

⏩

◀

▶

Back

Close

Full Screen / Esc

Printer-friendly Version

Interactive Discussion



which are not representative of any physical pattern variability. In the study of a climate network, it is preferable to filter out such weakly modular regions because partitioning them into communities could be misleading. Because (i) the detected Infomap partition is less affected by this filtration process than the modularity-based partitions and (ii) the fact that the random walkers in the Infomap algorithm are closely related to the flow in a dynamical network, the Infomap algorithm appears to be the best choice for the study of patterns of climate variability.

As representations of spatial patterns of variability, the communities of the network can be compared to EOFs. To assess the potential similarities and improvements brought by the detection of communities compared to EOFs, an EOF analysis was also conducted on the same data as used to build the H-SST network. EOF and rotated EOFs (R-EOFs) analysis of SST fields have been used by, e.g. Weare (1976) and Kawamura (1994), respectively. The first 6 EOFs of the SST field are shown in Fig. 4 and the R-EOFs using these 6 EOFs in Fig. 5. The R-EOFs are linear combinations of the 6 initial EOFs maximizing a given simplicity function or criterion, here the normalized varimax criterion of Kaiser (1958). Note that the eigenvector decomposition in the EOF analysis is based on the same correlations used to build the H-SST network. When the correlation matrix is used (and not the covariance matrix), every node is given the same weight without regard to their variance. We can see (Fig. 4) that only the first EOF can be associated to a community. The higher order EOF modes cannot be associated to any communities and they do not appear to represent any physical pattern of variability. On the contrary, the first 6 rotated EOFs can be associated with the dominant communities (Fig. 5). However, even higher order rotated-EOFs are very noisy and cannot be associated with any communities or known physical pattern of variability.

3.2 Communities in the H-SST network: interpretation

In this section, a physical interpretation of the communities of the H-SST network (Fig. 2b) is given. Community #1 is by far the dominant community in terms of

Network view of SST variability

A. Tantet and
H. A. Dijkstra

Title Page

Abstract

Introduction

Conclusions

References

Tables

Figures



Back

Close

Full Screen / Esc

Printer-friendly Version

Interactive Discussion



PageRank (69%) and size. Most of the nodes are in the tropical Pacific but remote patches – in the Pacific extra-tropics, tropical Indian ocean and northwestern tropical Atlantic – are also part of the community. This result suggests that teleconnections exist between the tropical Pacific and remote regions over the globe. These teleconnections can be deduced from the first-neighbour map which is plotted in Fig. 3a for community #1. For each node in the network, this map shows to which percentage of the nodes in the community it is connected to. For example, a node in the equatorial Atlantic is connected to about 25% of the nodes in the community.

From Fig. 3a, it can be seen that community #1 is well defined (nodes inside the community are connected to most of the other nodes of this community and are only sparsely connected to nodes outside the community) and that the different remote patches of the community are connected to each other. We have verified that the equatorial Pacific nodes are anti-correlated with those of the two small patches located around 30° in the North and South Pacific and to those near New-Zealand while they are positively correlated with the other nodes of the community. The spatial pattern of the community #1 also coincides with the EOF and R-EOF (Figs. 4a and 5a, respectively), explaining most of the variance. It also corresponds with the (December–February) El Niño-La Niña composites of HadISST SST determined in Alexander and Bladé (2002) (their Fig. 6a). These results suggest that the community #1 is representative of the dominant pattern of variability on interannual time-scales, i.e. ENSO.

The teleconnections shown in Fig. 3a have been described extensively in the literature. Perhaps the most well known remote impacts of ENSO are the changed atmospheric circulation over the northern Pacific and North America region and the associated SST anomalies in the North Pacific (Wallace and Gutzler, 1980; Deser and Blackmon, 1995; Lau, 1997). A similar relationship between the tropical and the South Pacific (Liu et al., 2002; Ciasto and Thompson, 2008) as well as the warming of the tropical Indian ocean (Lanzante, 1996; Klein et al., 1999) and tropical Atlantic (Curtis and Hastenrath, 1995; Lanzante, 1996; Enfield and Mayer, 1997; Klein et al., 1999) basins have also been reported. Previous studies suggest that the main mechanism in-

volved in these teleconnections on interannual time scales is the “atmospheric bridge” Lau and Nath (1996). This bridge occurs through changes in the Hadley and Walker cells and through the interaction of Rossby waves with the quasi-stationary flow and storm tracks (Trenberth et al., 1998; Alexander and Bladé, 2002).

Community #2, in terms of PageRank, is in the northern Atlantic. None of the EOFs in Fig. 4 resemble this community but the third R-EOF (Fig. 4c) exhibits clear similarities with it. This spatial pattern bears the signature of the AMO Guan and Nigam (2009).

The next community, #3, covers the maritime continent and the Philippine and East China seas, a region below referred to as the Indian Ocean–West Pacific (IWP). The second R-EOF (Fig. 4b) has a similar pattern as this community although it also shows strong variance in the Indian ocean. The IWP is located at the confluence of the Pacific and Indian Oceans and connects the two oceans by the Indonesian Through Flow (ITF). Ramage (1968) has shown that the IWP is one of the greatest source of energy for the extratropical circulation. Deep convection takes place in this region and the overlying atmosphere is highly sensitive to changes in SST (see Qu et al., 2005, for a review). Interannual variability in this region can be largely understood in terms of Kelvin and Rossby waves generated by remote zonal winds along the Indian and Pacific equatorial regions as well as by changes in the volume transport of the Indonesian Throughflow.

Although the other communities (#4–#10) also exhibit similarities with known spatial patterns of variability, we will not discuss this as their PageRank is much lower than the first three communities. For example, communities #8 and #9 are in the region of the pathways of the northern Western Boundary Currents (Qiu, 2000; Frankignoul, 2001) and community #4 appears to connect the southern wind-driven gyres (Speich et al., 2002). The first 6 communities can be associated with the first 6 R-EOFs, however, when more EOFs are rotated, no additional pattern of variability can be identified (not shown here). Hence, the community analysis allows to detect more detailed features of SST variability in the climate system.

Network view of SST variability

A. Tantet and
H. A. Dijkstra

Title Page

Abstract

Introduction

Conclusions

References

Tables

Figures



Back

Close

Full Screen / Esc

Printer-friendly Version

Interactive Discussion



4 Decadal SST variability and its connection with the GMST

4.1 Observations

We have seen that the community structure of the H-SST network is dominated by the first one and related to ENSO variability on interannual time scales. In order to focus on decadal variability we build a new network following the same methodology as before but using low-pass filtered time series of SST with a cutoff period of 8 yr to filter out the 2 to 7 yr band usually attributed to ENSO. The threshold τ was set to 0.6 in order to only keep absolute correlations above the maximum p value of the 95 % significance levels calculated over the globe using the MBB method (see Sect. 2). The resulting network, below referred to as the H-SST-LP8y network, has an edge density of 0.087 which is about 30 % smaller than the edge density of the H-SST network.

The degree centrality and the community structure of the H-SST-LP8y network are plotted in Fig. 6a and b, respectively. Overall, the spatial patterns appear similar to those of the H-SST network but important differences exist in the tropics. First of all, the degrees of the nodes in the H-SST-LP8y network located in the tropical Pacific and Indian ocean have decreased significantly, compared to those in the H-SST network; in the extra-tropics the opposite effect occurs (Fig. 6a). Community #1 (Fig. 6b) of the H-SST-LP8y network (which exhibits a similar pattern as the ENSO community in the H-SST network) has a much lower PageRank (31 % versus 69 % in the H-SST network). This result is expected when interannual variability and, a fortiori, variability related to ENSO, is filtered out. A second important difference is that the nodes lying in the Indian Ocean are no longer part of the same community as the nodes of the tropical Pacific. They are, instead, part of the same community as the nodes in the IWP region (community #2 in the H-SST-LP8y network). Furthermore, this IWP community has a PageRank of 26 % which is comparable to the PageRank of the tropical Pacific community #1 (31 %). The community of the North Atlantic (community #3 in the H-SST-LP8y network) and the community of the southern wind-driven gyres (community #4 in the H-SST-LP8y network) also exhibit higher PageRanks (15 and 11 %, respectively).

Network view of SST variability

A. Tantet and
H. A. Dijkstra

Title Page

Abstract

Introduction

Conclusions

References

Tables

Figures



Back

Close

Full Screen / Esc

Printer-friendly Version

Interactive Discussion



respectively) than the corresponding communities in the H-SST network. These results indicate that important components of decadal variability are present in the Indian Ocean–West Pacific region and the North Atlantic.

In order to investigate the relationship between the spatial patterns of variability represented by the communities and the global mean state of the climate system, correlations were calculated between mean SST time series associated with each community (in both H-SST and H-SST-LP8y networks) and three indices of global mean surface temperature (GMST). The time series representing the SST of a specific community was calculated by spatially averaging the time series of the nodes of the community. The Global Surface Temperature Anomalies of the NOAA (Smith and Reynolds, 2005) averaged over land and ocean (GMST), land only (GLST) and ocean only (GOST) were used as indices of the mean state of the climate system. The indices were processed using the same methodology as for the H-SST and H-SST-LP8y datasets (1 and 8 yr, respectively, low-pass filtered detrended anomalies) and cover the period 1880–2011. The correlations between the time series of the communities and the indices for the H-SST and H-SST-LP8y networks are presented in Table 1 and Table 2, respectively. For each correlation, a 95 % confidence interval is given in brackets and correlations significant at the 95 % level in bold face. The confidence intervals and significance levels were estimated using the MBB method as described in Sect. 2.

From both tables Tables 1 and 2, it is found that each of the communities is more correlated with the GOST than with the GLST. Only the communities #1–#3 and #5 in the H-SST network (Table 1) are significantly correlated with the GLST. On decadal time-scales (Table 2), the first three communities also show significant correlations with the GLST but the ENSO community (#1) does not display the largest correlation to the GLST and to the GOST anymore (as in the H-SST network). Now the Indian Ocean–West Pacific community (#2) and the North Atlantic community (#3) are best correlated to the GOST with the Indian Ocean–West Pacific (IWP) community displaying largest correlations to the GLST. The correlations of 0.77 and 0.84 between the IWP time-

Network view of SST variability

A. Tantet and
H. A. Dijkstra

Title Page

Abstract

Introduction

Conclusions

References

Tables

Figures



Back

Close

Full Screen / Esc

Printer-friendly Version

Interactive Discussion



series of SST and GLST and GMST, respectively, is striking and the region of the Indian Ocean–West Pacific appears to play a major role in decadal climate variability.

In Fig. 7, the SST time series of both the Indian Ocean–West Pacific community, and the North Atlantic community are regressed against the GMST and GLST indices.

The fits of the time series of the two communities to the GMST and GLST result in coefficients of multiple-determination (von Storch and Zwiers, 1999b) of 0.87 and 0.66, respectively. This shows that the patterns of both communities can, together, explain most of the decadal variability of the GMST and the largest part of the decadal variability of the GLST. Also, the phase synchronization of the time series of both communities has contributed, to a large extent, to the increase in GMST since the 1970s (Fig. 7).

4.2 ESM simulations

As communities are able to distinguish patterns of climate variability in the HadISST data, the network methods also potentially offer a more detailed tool to assess the quality of state-of-the-art Earth System Models (ESMs) in simulating these patterns. To investigate this, SST fields from a three-member ensemble of historical simulations (1870–2005), obtained with the MPI-ESM-LR model (Jungclaus et al., 2013; Stevens and Giorgetta, 2013) for the CMIP5 project (Taylor et al., 2012), were used to reconstruct two networks following the same methodology as for the H-SST and H-SST-LP8y networks. These model networks will be referred to below as the ESM-SST and ESM-SST-LP8y networks, respectively.

The degree distribution and community structure of the ESM-SST network are plotted in Fig. 8a and b, respectively. Similar to the results for the H-SST network, the ENSO community (#1) and the IWP community (#3) are visible (Fig. 8b), the ENSO community dominating with a PageRank of 81 %. However, only the southern half of the North Atlantic community is present (community #5 in Fig. 8b), likely indicative of an under-representation of the AMO-related variability in the model. Also, fewer connections between the ENSO community and the extratropical Pacific are visible (Fig. 8a and b) than in the H-SST network. A weaker atmospheric bridge may be

Network view of SST variability

A. Tantet and
H. A. Dijkstra

Title Page

Abstract

Introduction

Conclusions

References

Tables

Figures



Back

Close

Full Screen / Esc

Printer-friendly Version

Interactive Discussion



responsible for the absence of such teleconnections. Finally, we can see in Table 3 that the ENSO, IWP and North Atlantic communities are, as in the observations, most strongly correlated to the GLST.

For the ESM-SST-LP8y network, the degree distribution and community structure (shown in Fig. 9a and b, respectively) are quite similar to those of the ESM-SST network. However, most of the nodes in the extra-tropics are orphan, indicative of a weak spatial coherence of the extratropical SST variability. Interestingly, the PageRank of the ENSO community (community #1) is still very high (81 %) so that decadal variability is also dominated by the ENSO community. This too strong decadal tropical variability has already been reported by Jungclaus and Keenlyside (2006) for a previous configuration of this model (ECHAM5/MPI-OM). Zanchettin et al. (2012) also showed that the tropical Indian SSTs are over-sensitive to tropical Pacific fluctuations in this model. Decadal variability in the GLST within this ESM can be largely explained by the ENSO and IWP communities, but misses the connection to the AMO as found in the observations (Table 4 and Fig. 10).

To conclude, the main aspects of the SST variability found in the observations are also visible in the MPI-ESM-LR model but the variability related to ENSO (AMO) is over-represented (under-represented). These model biases could be efficiently identified thanks to the network approach.

5 Summary and discussion

In order to study the global climate variability, we have analyzed SST observations and ESM simulations using a climate network approach focusing on the detection of communities. The network techniques provide an innovative and efficient complementary approach to more traditional methods like EOF analysis, composite analysis and correlation maps.

An EOF analysis is usually efficient in detecting the dominant mode of variability but the secondary modes, being constrained to be orthogonal to the first one, are less

Network view of SST variability

A. Tantet and
H. A. Dijkstra

Title Page

Abstract

Introduction

Conclusions

References

Tables

Figures



Back

Close

Full Screen / Esc

Printer-friendly Version

Interactive Discussion



Network view of SST variability

A. Tantet and
H. A. Dijkstra

Title Page

Abstract

Introduction

Conclusions

References

Tables

Figures



Back

Close

Full Screen / Esc

Printer-friendly Version

Interactive Discussion



likely to represent regional patterns of variability Monahan et al. (2009). Thus, when applying an EOF analysis on the HadISST SST data over the globe, only the first EOF can be attributed to a physical pattern of climate variability, namely ENSO, while the higher EOF modes could not be connected to any known patterns of variability.

This shortcoming can be overcome by rotating the EOFs like was done by Kawamura (1994). However, one of the drawbacks of this method is that the results are sensitive to the choice of the rotation criterion, to the choice of the number of loadings and to the normalization of the EOFs (von Storch and Zwiers, 1999a).

On the contrary, when calculating the degree centrality of the nodes of a network, the connections between nodes are evaluated without respect to any specific mode or direction in the space of the nodes, allowing for the coexistence of different modes of variability. This explains why patterns of variability not, or weakly, related to ENSO are also apparent in the degree distribution of the H-SST network (Fig. 1). However, contrary to an EOF analysis, the degree centrality does not allow to distinguish different patterns of variability from one another. Thus, a community analysis must subsequently be applied to distribute the nodes into distinct groups of covarying nodes.

Finding communities in a network is a much more efficient way to reveal non-overlapping spatial patterns of variability of the global climate system than an EOF analysis. We have indeed shown in Sect. 3 that most of the communities in the H-SST network (Fig. 2) can be associated to known physical patterns of variability, which could not have been done using a regular EOF analysis on the global oceans. More patterns could be found using 6 rotated EOFs but the choice of the number of loadings could only be done by evaluating the correspondence of the rotated EOFs with the communities. However, the main drawback of the Infomap community detection algorithm is that it is not able to detect overlapping spatial patterns of variability. For example, we can see from Fig. 3 that the nodes in the Caribbean Sea associated with the second community (#2) could also be associated with the first community which was also suggested by Guan and Nigam (2009). Overlapping community detection algorithms exist (e.g. Shen et al., 2009; Lancichinetti et al., 2009), however, because of their complex

implementation and slower execution application of these techniques are outside the scope of this study.

By augmenting the community analysis with first neighbours maps (Fig. 3), teleconnections and links between communities can be revealed. The study of these maps offers several advantages over correlation maps or composites. The main interest of the network approach is that neither a statistical event nor an index has to be defined a priori. For example, the results obtained using the first neighbours of the ENSO community in the H-SST network (Fig. 3a) are similar to those of Alexander and Bladé (2002) using composites, but we did not need to define what El Niño and La Niña events represent statistically. Correlation maps obtained by Klein et al. (1999) and Alexander and Bladé (2002) are also similar to Fig. 3a, but once again, we did not need to define over which domain to spatially average to obtain the relevant time series. In short, thanks to the community detection algorithm, neither prior information nor a choice of a pattern of variability to be studied is necessary, making pioneering studies easier and maybe also less biased.

The community structure of the H-SST network (Fig. 2) proved to be in good agreement with known spatial patterns of climate variability, further supporting the use of this method to identify climate patterns of variability from large gridded datasets. On inter-annual time-scales, the main community could be associated with the dominant pattern of variability, ENSO and its remote influences were visible as part of the community or in the first neighbour maps. These teleconnections could in part be interpreted using the “atmospheric bridge” concept. Other patterns of variability, such as the AMO, were also visible as independent components of the system.

One of the key differences between the H-SST and the H-SST-LP8y networks is that the Indian Ocean–West Pacific (IWP) region appears an independent and strongly intra-connected community in the H-SST-LP8y network whereas it’s western part is connected to the tropical Pacific in the H-SST network. This suggests that decadal variability in the IWP region is not driven by tropical Pacific variability through the atmospheric bridge as on interannual time-scales. Furthermore, a large component of the

Network view of SST variability

A. Tantet and
H. A. Dijkstra

Title Page

Abstract

Introduction

Conclusions

References

Tables

Figures

◀

▶

◀

▶

Back

Close

Full Screen / Esc

Printer-friendly Version

Interactive Discussion



Network view of SST variability

A. Tantet and
H. A. Dijkstra

Title Page

Abstract

Introduction

Conclusions

References

Tables

Figures

◀

▶

◀

▶

Back

Close

Full Screen / Esc

Printer-friendly Version

Interactive Discussion



- Barthélemy, M.: Spatial networks, *Physics Reports*, 499, 1–101, doi:j.physrep.2010.11.002, 2011. 749
- Bindoff, N. and McDougall, T.: Decadal changes along an Indian Ocean Section at 32° S and their interpretation, *J. Phys. Oceanogr.*, 30, 1207–1222, 2000. 762
- 5 Blondel, V. D., Guillaume, J.-L., Lambiotte, R., and Lefebvre, E.: Fast unfolding of communities in large networks, *J. Stat. Mech. Theor. Exp.*, 2008, P10008, doi:10.1088/1742-5468/2008/10/P10008, 2008. 750
- Brin, S. and Page, L.: The anatomy of a large-scale hypertextual Web search engine, *Computer Netw. ISDN Syst.*, 30, 107–117, doi:10.1016/S0169-7552(98)00110-X, 1998. 751
- 10 Ciasto, L. M. and Thompson, D. W. J.: Observations of Large-Scale Ocean–Atmosphere Interaction in the Southern Hemisphere, *J. Climate*, 21, 1244–1259, doi:10.1175/2007JCLI1809.1, 2008. 754
- Costa, L. and Rodrigues, F.: Characterization of complex networks: a survey of measurements, *Adv. Phys.*, 56, 167–242, 2007. 749
- 15 Curtis, S. and Hastenrath, S.: Forcing of anomalous sea surface temperature evolution in the tropical Atlantic during Pacific warm events, *J. Geophys. Res.*, 100, 15835–15847, 1995. 754
- Delworth, T.: GFDL’s CM2 Global Coupled Climate Models, Part I: Formulation and simulation characteristics, *J. Climate*, 19, 643–674, 2006. 750
- Deser, C. and Blackmon, M.: On the relationship between tropical and north Pacific sea surface temperature variations, *J. Climate*, 8, 1677–1680, 1995. 754
- 20 Deser, C., Alexander, M. A., Xie, S.-P., and Phillips, A. S.: Sea surface temperature variability: patterns and mechanisms, *Annu. Rev. Mar. Sci.*, 2, 115–143, doi:10.1146/annurev-marine-120408-151453, 2010. 745
- Dommenget, D.: The Ocean’s role in continental climate variability and change, *J. Climate*, 22, 4939–4952, doi:10.1175/2009JCLI2778.1, 2009. 762
- 25 Dommenget, D. and Latif, M.: Generation of hyper climate modes, *Geophys. Res. Lett.*, 35, L02706, doi:10.1029/2007GL031087, 2008. 763
- Donges, J. F., Zou, Y., Marwan, N., and Kurths, J.: Complex networks in climate dynamics, *Eur. Phys. J. Spec. Top.*, 174, 157–179, doi:10.1140/epjst/e2009-01098-2, 2009a. 745
- 30 Donges, J. F., Zou, Y., Marwan, N., and Kurths, J.: The backbone of the climate network, *Europhys. Lett.*, 87, 48007, doi:10.1209/0295-5075/87/48007, 2009b. 745

**Network view of SST
variability**A. Tantet and
H. A. Dijkstra

Title Page

Abstract

Introduction

Conclusions

References

Tables

Figures

◀

▶

◀

▶

Back

Close

Full Screen / Esc

Printer-friendly Version

Interactive Discussion



- Donges, J. F., Schultz, H. C. H., Marwan, N., Zou, Y., and Kurths, J.: Investigating the topology of interacting networks, *Eur. Phys. J. B*, 84, 635–651, doi:10.1140/epjb/e2011-10795-8, 2011. 746
- Duchon, C.: Lanczos filtering in one and two dimensions, *J. Appl. Meteorol.*, 18, 1016–1022, doi:10.1175/1520-0450(1979)018<1016:LFIOAT>2.0.CO;2, 1979. 747
- Enfield, D.: The Atlantic multidecadal oscillation and its relation to rainfall and river flows in the continental US, *Geophys. Res. Lett.*, 28, 2077–2080, 2001. 745
- Enfield, D. and Mayer, D.: Tropical Atlantic sea surface temperature variability relation to El Niño-Southern Oscillation, *J. Geophys. Res.*, 102, 929–945, 1997. 754
- Frankignoul, C.: Gulf stream variability and Ocean–Atmosphere interactions, *J. Phys. Oceanogr.*, 31, 3516–3529, 2001. 755
- Gozolchiani, A., Yamasaki, K., Gazit, O., and Havlin, S.: Pattern of climate network blinking links follows El Niño events, *Europhys. Lett.*, 83, 28005, doi:10.1209/0295-5075/83/28005, 2008. 746
- Gozolchiani, A., Havlin, S., and Yamasaki, K.: Emergence of El Niño as an autonomous component in the climate network, *Phy. Rev. Lett.*, 107, 1–5, doi:10.1103/PhysRevLett.107.148501, 2011. 746
- Guan, B. and Nigam, S.: Analysis of Atlantic SST variability factoring interbasin links and the secular trend: clarified structure of the Atlantic Multidecadal Oscillation, *J. Climate*, 22, 4228–4240, doi:10.1175/2009JCLI2921.1, 2009. 755, 760
- Hasselmann, K.: Stochastic climate models Part I. Theory, *Tellus*, 28, 473–485, doi:10.1111/j.2153-3490.1976.tb00696.x, 1976. 762
- Hu, Z.-Z.: Interdecadal variability of summer climate over East Asia and its association with 500 hPa height and global sea surface temperature, *J. Geophys. Res.*, 102, 19403, doi:10.1029/97JD01052, 1997. 762
- Jungclaus, J. H. and Keenlyside, N.: Ocean circulation and tropical variability in the coupled model ECHAM5/MPI-OM, *J. Climate*, 19, 3952–3972, 2006. 759
- Jungclaus, J. H., Fischer, N., Haak, H., Lohmann, K., Marotzke, J., Matei, D., Mikolajewicz, U., Notz, D., and von Storch, J.: Characteristics of the ocean simulations in MPIOM, the ocean component of the MPI-Earth system model, *J. Adv. Model. Earth Syst.*, 5, 422–446, doi:10.1002/jame.20023, 2013. 758
- Kaiser, H.: The varimax criterion for analytic rotation in factor analysis, *Psychometrika*, 23, 187–200, 1958. 753

Network view of SST variability

A. Tantet and
H. A. Dijkstra

Title Page

Abstract

Introduction

Conclusions

References

Tables

Figures

◀

▶

◀

▶

Back

Close

Full Screen / Esc

Printer-friendly Version

Interactive Discussion



- Kawamura, R.: A rotated eof analysis of global sea surface temperature variability with interannual interdecadal scales, *J. Phys. Oceanogr.*, 24, 707–715, 1994. 753, 760
- Kistler, R., Kalnay, E., and Collins, W.: The NCEP-NCAR 50-year reanalysis: monthly means CD-ROM and documentation, *B. Am. Meteorol. Soc.*, 82, 247–268, 2001. 750
- 5 Klein, S., Soden, B., and Lau, N.: Remote sea surface temperature variations during ENSO: evidence for a tropical atmospheric bridge, *J. Climate*, 12, 917–932, 1999. 754, 761
- Lancichinetti, A. and Fortunato, S.: Community detection algorithms: a comparative analysis, *Phys. Rev. E*, 80, 1–11, doi:10.1103/PhysRevE.80.056117, 2009. 750
- Lancichinetti, A., Fortunato, S., and Kertész, J.: Detecting the overlapping and hierarchical
10 community structure in complex networks, *New J. Phys.*, 11, 033015, doi:10.1088/1367-2630/11/3/033015, 2009. 760
- Lanzante, J.: Lag relationship involving sea surface temperatures, *J. Climate*, 9, 2568–2578, 1996. 754
- Lau, N.-C.: Interactions between Global SST Anomalies and the Midlatitude Atmospheric Circulation, *B. Am. Meteorol. Soc.*, 78, 21–33, doi:10.1175/1520-0477(1997)078<0021:IBGSAA>2.0.CO;2, 1997. 754
- Lau, N.-C. and Nath, M.: The role of the “Atmospheric Bridge” in linking tropical pacific ENSO events to extratropical SST anomalies, *J. Climate*, 9, 2036–2057, 1996. 755
- Lee, T.: Decadal weakening of the shallow overturning circulation in the South Indian Ocean,
20 *Geophys. Res. Lett.*, 31, L18305, doi:10.1029/2004GL020884, 2004. 762
- Liu, J., Yuan, X., Rind, D., and Martinson, D.: Mechanism study of the ENSO and southern high latitude climate teleconnections, *Geophys. Res. Lett.*, 29, 8–11, 2002. 754
- McDonagh, E. and Bryden, H.: Decadal changes in the South Indian Ocean thermocline, *J. Climate*, 18, 1575–1590, 2005. 762
- 25 McPhaden, M. J., Busalacchi, J., Cheney, R., Gage, S., Halpern, D., Ji, M., Julian, P., Mitchurn, G. T., Niiler, P. P., and Smith, N.: The tropical Ocean–global atmosphere observing system: a decade of progress, *J. Geophys. Res.*, 103, 14169–14240, 1998. 745
- Monahan, A. H., Fyfe, J. C., Ambaum, M. H. P., Stephenson, D. B., and North, G. R.: Empirical orthogonal functions: the medium is the message, *J. Climate*, 22, 6501–6514, 2009. 745,
30 760
- Mudelsee, M.: *Climate Time Series Analysis: Classical Statistical and Bootstrap Methods*, available at: <http://books.google.com/books?hl=en&lr=&id=eqmoGuN4SH4C&oi=fnd&pg=PR7&dq=Climate+Time+Series+Analysis:+Classical+Statistical+and+Bootstrap+>

Network view of SST variability

A. Tantet and
H. A. Dijkstra

Title Page

Abstract

Introduction

Conclusions

References

Tables

Figures



Back

Close

Full Screen / Esc

Printer-friendly Version

Interactive Discussion



Methods.ots=4yKbmCHgxs&sig=sUdqodwqQuv5oBY2LFZVwmh-Cw0, Atmospheric and Oceanographic Sciences Library, Springer, 2010. 748

Muller, R. a., Curry, J., Groom, D., Jacobsen, R., Perlmutter, S., Rohde, R., Rosenfeld, A., Wickham, C., and Wurtele, J.: Decadal variations in the global atmospheric land temperatures, *J. Geophys. Res.-Atmos.*, 118, 5280–5286, doi:10.1002/jgrd.50458, 2013. 745

Newman, M. E. J.: Finding community structure in networks using the eigenvectors of matrices, *Phys. Rev. E*, 74, 036104, doi:10.1103/PhysRevE.74.036104, 2006. 750

Newman, M. E. J. and Girvan, M.: Finding and evaluating community structure in networks, *Phys. Rev. E*, 69, 1–15, doi:10.1103/PhysRevE.69.026113, 2004. 750, 751

Qiu, B.: Interannual variability of the Kuroshio Extension system and its impact on the wintertime SST field, *J. Phys. Oceanogr.*, 30, 1486–1502, 2000. 755

Qu, T., Du, Y., Strachan, J., Meyers, G., and Slingo, J.: Sea surface temperature and its variability in the Indonesian region, *Oceanography*, 18, 50–61, 2005. 755

Ramage, C.: Role of a tropical maritime continent in the atmospheric circulation, *Mon. Weather Rev.*, 96, 365–370, 1968. 755

Rayner, N. A.: Global analyses of sea surface temperature, sea ice, and night marine air temperature since the late nineteenth century, *J. Geophys. Res.*, 108, 4407, doi:10.1029/2002JD002670, 2003. 746

Rosvall, M. and Bergstrom, C.: An information-theoretic framework for resolving community structure in complex networks, *P. Natl. Acad. Sci. USA*, 104, 7327–7331, 2007. 750

Shen, H., Cheng, X., Cai, K., and Hu, M.-B.: Detect overlapping and hierarchical community structure in networks, *Physica A*, 388, 1706–1712, doi:10.1016/j.physa.2008.12.021, 2009. 760

Smith, T. and Reynolds, R.: A global merged land-air-sea surface temperature reconstruction based on historical observations (1880–1997), *J. Climate*, 18, 2021–2036, 2005. 757

Speich, S., Blanke, B., and Vries, P. D.: Tasman leakage: a new route in the global ocean conveyor belt, *Geophys. Res. Lett.*, 29, 1–4, 2002. 755

Stevens, B. and Giorgetta, M.: The atmospheric component of the MPI-M earth system model: ECHAM6, *J. Adv. Model. Earth Syst.*, 5, 1–83, 2013. 758

Sutton, R. T. and Hodson, D. L. R.: Atlantic Ocean forcing of North American and European summer climate, *Science*, 309, 115–8, doi:10.1126/science.1109496, 2005. 745

Network view of SST variability

A. Tantet and
H. A. Dijkstra

Title Page

Abstract

Introduction

Conclusions

References

Tables

Figures

◀

▶

◀

▶

Back

Close

Full Screen / Esc

Printer-friendly Version

Interactive Discussion



- Sutton, R. T., Dong, B., and Gregory, J. M.: Land/sea warming ratio in response to climate change: IPCC AR4 model results and comparison with observations, *Geophys. Res. Lett.*, 34, L02701, doi:10.1029/2006GL028164, 2007. 744
- Trenberth, K. E.: The definition of El Nino, *B. Am. Meteorol. Soc.*, 78, 2771–2777, 1997. 745
- 5 Taylor, K. E., Stouffer, R. J., and Meehl, G. A.: An overview of CMIP5 and the experiment design, *B. Am. Meteorol. Soc.*, 93, 485–498, doi:10.1175/BAMS-D-11-00094.1, 2012. 758
- Trenberth, K. E., Branstator, G. W., Karoly, D., Kumar, A., Lau, N.-C., and Ropelewski, C.: Progress during TOGA in understanding and modeling global teleconnections associated with tropical sea surface temperatures, *J. Geophys. Res.*, 103, 14291, doi:10.1029/97JC01444, 1998. 755
- 10 Tsonis, A. A. and Roebber, P.: The architecture of the climate network, *Physica A*, 333, 497–504, doi:10.1016/j.physa.2003.10.045, 2004. 745, 746, 747, 750
- Tsonis, A. A. and Swanson, K.: Topology and predictability of El Niño and La Niña networks, *Phys. Rev. Lett.*, 100, 228502, doi:10.1103/PhysRevLett.100.228502, 2008. 746
- 15 Tsonis, A. A., Swanson, K., and Kravtsov, S.: A new dynamical mechanism for major climate shifts, *Geophys. Res. Lett.*, 34, 1–5, doi:10.1029/2007GL030288, 2007. 746
- Tsonis, A. A., Swanson, K. L., and Wang, G.: On the role of atmospheric teleconnections in climate, *J. Climate*, 21, 2990–3001, doi:10.1175/2007JCLI1907.1, 2008. 745
- 20 Tsonis, A. A., Wang, G., Swanson, K. L., Rodrigues, F. A., and Costa, L. D. F.: Community structure and dynamics in climate networks, *Clim. Dynam.*, 37, 933–940, doi:10.1007/s00382-010-0874-3, 2010. 745, 746, 747, 750
- Valsala, V., Maksyutov, S., and Murtugudde, R.: Possible interannual to interdecadal variabilities of the Indonesian throughflow water pathways in the Indian Ocean, *J. Geophys. Res.*, 115, C10016, doi:10.1029/2009JC005735, 2010. 762
- 25 von Storch, H. and Zwiers, F. W.: Empirical orthogonal functions, in: *Statistical Analysis in Climate Research*, chap. 13, Cambridge University Press, 293–316, doi:10.1017/CBO9780511612336.014, 1999a. 745, 760
- von Storch, H. and Zwiers, F. W.: Regression, in: *Statistical Analysis in Climate Research*, chap. 8, Cambridge University Press, 145–169, doi:10.1017/CBO9780511612336.014, 1999b. 758
- 30 Wallace, J. and Gutzler, D. S.: Teleconnections in the geopotential height field during the Northern Hemisphere winter, *Mon. Weather Rev.*, 109, 784–812, 1980. 754

Network view of SST variability

A. Tantet and
H. A. Dijkstra

Title Page

Abstract

Introduction

Conclusions

References

Tables

Figures

◀

▶

◀

▶

Back

Close

Full Screen / Esc

Printer-friendly Version

Interactive Discussion



Wang, C., Xie, S. P., and Carton, J. A.: A global survey of ocean-atmosphere interaction and climate variability, in: Earth Climate: The Ocean-Atmosphere Interaction Geophysical Monograph, American Geophysical Union, 1–19, 2004. 745

Weare, B.: Empirical orthogonal analysis of Pacific sea surface temperature, *J. Phys. Oceanogr.*, 6, 671–678, 1976. 753

Wyatt, M. G., Kravtsov, S., and Tsonis, A. A.: Atlantic Multidecadal Oscillation and Northern Hemisphere's climate variability, *Clim. Dynam.*, 38, 929–949, doi:10.1007/s00382-011-1071-8, 2011. 746

Yamasaki, K., Gozolchiani, A., and Havlin, S.: Climate networks around the globe are significantly affected by El Niño, *Phys. Rev. Lett.*, 100, 1–4, doi:10.1103/PhysRevLett.100.228501, 2008. 746

Zanchettin, D., Rubino, A., Matei, D., Bothe, O., and Jungclaus, J. H.: Multidecadal-to-centennial SST variability in the MPI-ESM simulation ensemble for the last millennium, *Clim. Dynam.*, 40, 1301–1318, doi:10.1007/s00382-012-1361-9, 2012. 759

Zhang, Y., Li, T., and Wang, B.: Decadal change of the spring snow depth over the Tibetan Plateau: the associated circulation and influence on the East Asian summer monsoon, *J. Climate*, 17, 2780–2793, 2004. 762

Zhou, T., Yu, R., Zhang, J., Drange, H., Cassou, C., Deser, C., Hodson, D. L. R., Sanchez-Gomez, E., Li, J., Keenlyside, N., Xin, X., and Okumura, Y.: Why the western Pacific subtropical high has extended westward since the late 1970s, *J. Climate*, 22, 2199–2215, doi:10.1175/2008JCLI2527.1, 2009. 762

Network view of SST variability

A. Tantet and
H. A. Dijkstra

Table 1. Correlations between the mean time series of the communities of the H-SST network and the indices of mean, land and ocean surface temperatures (all time series 1y low-pass filtered). 95 % confidence intervals are given in brackets and correlations significant at 95 % in bold face.

#	GMST	GLST	GOST
1	0.66 [0.62, 0.73]	0.44 [0.36, 0.51]	0.71 [0.67, 0.79]
2	0.59 [0.43, 0.68]	0.43 [0.19, 0.55]	0.59 [0.47, 0.68]
3	0.50 [0.30, 0.54]	0.44 [0.23, 0.50]	0.45 [0.24, 0.52]
4	0.41 [0.13, 0.50]	0.22 [−0.06, 0.35]	0.45 [0.21, 0.54]
5	0.42 [0.33, 0.54]	0.30 [0.18, 0.42]	0.43 [0.34, 0.53]
6	0.25 [0.07, 0.40]	0.11 [−0.06, 0.24]	0.30 [0.11, 0.46]
7	0.26 [0.11, 0.44]	0.11 [−0.02, 0.21]	0.32 [0.16, 0.52]
8	0.22 [0.02, 0.35]	0.17 [−0.07, 0.35]	0.21 [0.02, 0.32]
9	0.14 [−0.18, 0.37]	0.07 [−0.29, 0.35]	0.16 [−0.08, 0.32]
10	0.27 [0.05, 0.37]	0.07 [−0.12, 0.18]	0.35 [0.12, 0.45]

[Title Page](#)
[Abstract](#)
[Introduction](#)
[Conclusions](#)
[References](#)
[Tables](#)
[Figures](#)
[◀](#)
[▶](#)
[◀](#)
[▶](#)
[Back](#)
[Close](#)
[Full Screen / Esc](#)
[Printer-friendly Version](#)
[Interactive Discussion](#)


Network view of SST variability

A. Tantet and
H. A. Dijkstra

Title Page

Abstract

Introduction

Conclusions

References

Tables

Figures

◀

▶

◀

▶

Back

Close

Full Screen / Esc

Printer-friendly Version

Interactive Discussion



Table 2. Correlations between the mean time series of the communities of the H-SST-LP8y network and the indices of mean, land and ocean surface temperatures (all time series 8y low-pass filtered). 95% confidence intervals are given in brackets and correlations significant at 95% in bold face.

#	GMST	GLST	GOST
1	0.52 [0.36, 0.73]	0.47 [0.28, 0.68]	0.50 [0.33, 0.66]
2	0.84 [0.72, 0.91]	0.77 [0.55, 0.89]	0.78 [0.59, 0.87]
3	0.65 [0.38, 0.83]	0.49 [0.06, 0.77]	0.67 [0.43, 0.82]
4	0.55 [0.18, 0.74]	0.28 [−0.22, 0.56]	0.62 [0.33, 0.78]
5	0.35 [−0.15, 0.59]	0.29 [−0.24, 0.57]	0.34 [−0.11, 0.56]
6	0.45 [0.18, 0.62]	0.34 [0.02, 0.59]	0.44 [0.18, 0.61]
7	0.51 [0.30, 0.77]	0.19 [−0.06, 0.47]	0.63 [0.39, 0.85]
8	0.55 [0.16, 0.69]	0.24 [−0.23, 0.44]	0.64 [0.25, 0.75]
9	0.12 [−0.37, 0.49]	0.04 [−0.53, 0.56]	0.14 [−0.27, 0.44]
10	−0.14 [−0.53, 0.29]	−0.51 [−0.70, −0.12]	0.07 [−0.43, 0.44]

Network view of SST variability

A. Tantet and
H. A. Dijkstra

Table 3. Correlations between the mean time series of the communities of the ESM-SST network and the indices of mean, land and ocean surface temperatures (all time series 1y low-pass filtered). 95 % confidence intervals are given in brackets and correlations significant at 95 % are bold face.

#	GMST	GLST	GOST
1	0.63 [0.56, 0.67]	0.65 [0.56, 0.69]	0.67 [0.61, 0.71]
2	0.68 [0.58, 0.71]	0.41 [0.25, 0.45]	0.47 [0.32, 0.51]
3	0.42 [0.26, 0.45]	0.38 [0.21, 0.41]	0.38 [0.22, 0.42]
4	0.35 [0.18, 0.41]	0.34 [0.19, 0.40]	0.33 [0.16, 0.40]
5	0.44 [0.31, 0.50]	0.44 [0.31, 0.49]	0.49 [0.36, 0.56]
6	-0.05 [-0.19, 0.01]	-0.11 [-0.22, -0.03]	-0.04 [-0.18, 0.04]
7	0.31 [0.18, 0.36]	0.33 [0.21, 0.38]	0.30 [0.16, 0.36]
8	0.33 [0.17, 0.38]	0.30 [0.17, 0.35]	0.35 [0.21, 0.39]
9	0.16 [-0.05, 0.23]	0.14 [-0.03, 0.21]	0.13 [-0.08, 0.20]
10	0.16 [0.00, 0.20]	0.18 [0.04, 0.23]	0.14 [-0.02, 0.20]
11	0.14 [-0.15, 0.21]	0.10 [-0.14, 0.19]	0.11 [-0.16, 0.18]
12	0.40 [0.24, 0.47]	0.39 [0.25, 0.43]	0.43 [0.28, 0.49]

[Title Page](#)
[Abstract](#)
[Introduction](#)
[Conclusions](#)
[References](#)
[Tables](#)
[Figures](#)
[Back](#)
[Close](#)
[Full Screen / Esc](#)
[Printer-friendly Version](#)
[Interactive Discussion](#)


Network view of SST variability

A. Tantet and
H. A. Dijkstra

Table 4. Correlations between the mean time series of the communities of the ESM-SST-LP8y network and the indices of mean, land and ocean surface temperatures (all time series 8y low-pass filtered). 95 % confidence intervals are given in brackets and correlations significant at 95 % in bold face.

#	GMST	GLST	GOST
1	0.68 [0.51, 0.74]	0.75 [0.60, 0.80]	0.68 [0.50, 0.73]
2	0.60 [0.36, 0.67]	0.66 [0.44, 0.73]	0.62 [0.38, 0.70]
3	0.75 [0.55, 0.77]	0.75 [0.55, 0.78]	0.69 [0.46, 0.72]
4	0.77 [0.55, 0.80]	0.63 [0.29, 0.67]	0.62 [0.30, 0.67]
5	0.46 [0.13, 0.52]	0.48 [0.21, 0.53]	0.48 [0.18, 0.54]

[Title Page](#)
[Abstract](#)
[Introduction](#)
[Conclusions](#)
[References](#)
[Tables](#)
[Figures](#)
[Back](#)
[Close](#)
[Full Screen / Esc](#)
[Printer-friendly Version](#)
[Interactive Discussion](#)

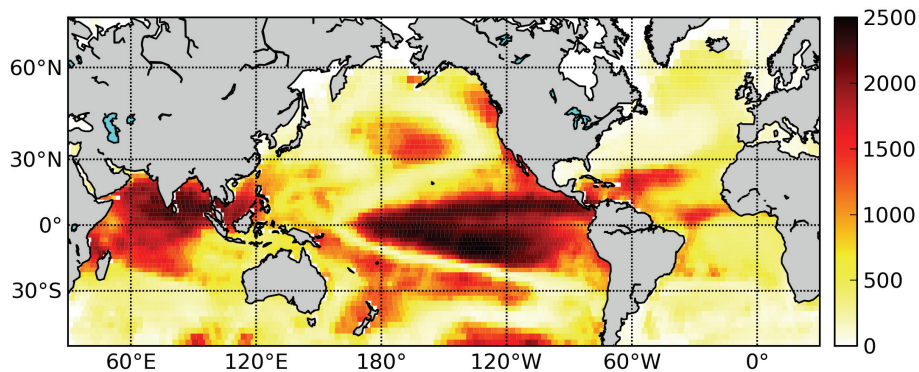

Network view of SST variabilityA. Tantet and
H. A. Dijkstra

Fig. 1. Degree centrality, as defined by Eq. (3), of the nodes of the H-SST network. A threshold $\tau = 0.4$ was used to construct the network giving an edge density $\rho = 0.14$.

Title Page

Abstract

Introduction

Conclusions

References

Tables

Figures

◀

▶

◀

▶

Back

Close

Full Screen / Esc

Printer-friendly Version

Interactive Discussion



Network view of SST variability

A. Tantet and
H. A. Dijkstra

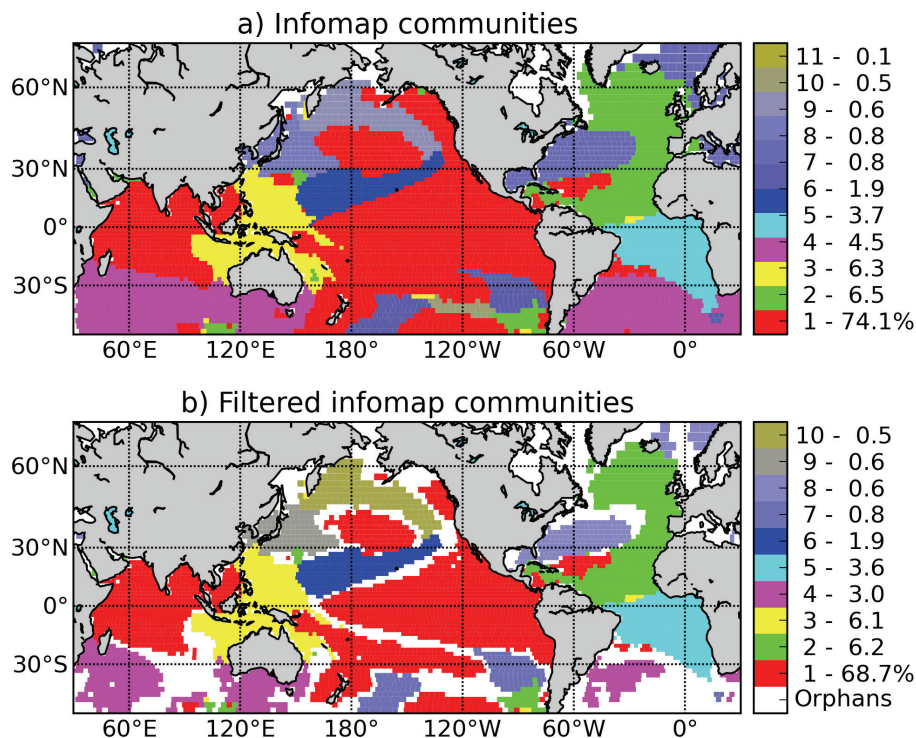


Fig. 2. (a) Infomap communities in the H-SST network. Each color represents one community and each node is assigned the color of the community it belongs to. The communities are ordered by decreasing total PageRank of their nodes which is written to the right of the scale. (b) Infomap communities after filtration of nodes which are connected to a fraction of their community smaller than twice the density of the network or belong to communities with nodes smaller than 2 % of the network. Nodes in white are orphans, they do not belong to any community.

[Title Page](#)
[Abstract](#)
[Introduction](#)
[Conclusions](#)
[References](#)
[Tables](#)
[Figures](#)
[Back](#)
[Close](#)
[Full Screen / Esc](#)
[Printer-friendly Version](#)
[Interactive Discussion](#)

Network view of SST variability

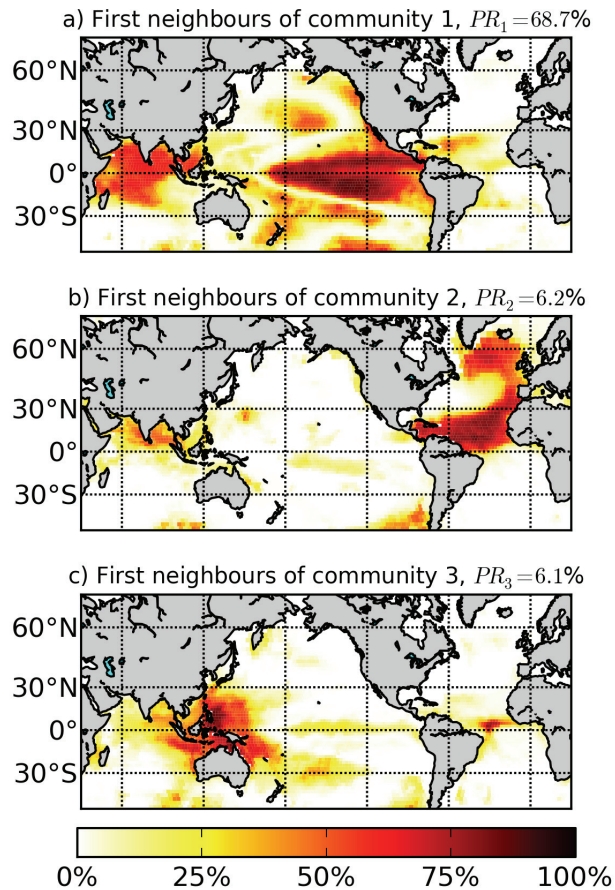
A. Tantet and
H. A. Dijkstra

Fig. 3. First neighbours map of communities (a) #1, (b) #2, and (c) #3 in the H-SST network. For each node, the color scale indicates the percentage of the nodes in the community to which that node is connected.

Title Page

Abstract

Introduction

Conclusions

References

Tables

Figures

◀

▶

◀

▶

Back

Close

Full Screen / Esc

Printer-friendly Version

Interactive Discussion



Network view of SST variability

A. Tantet and
H. A. Dijkstra

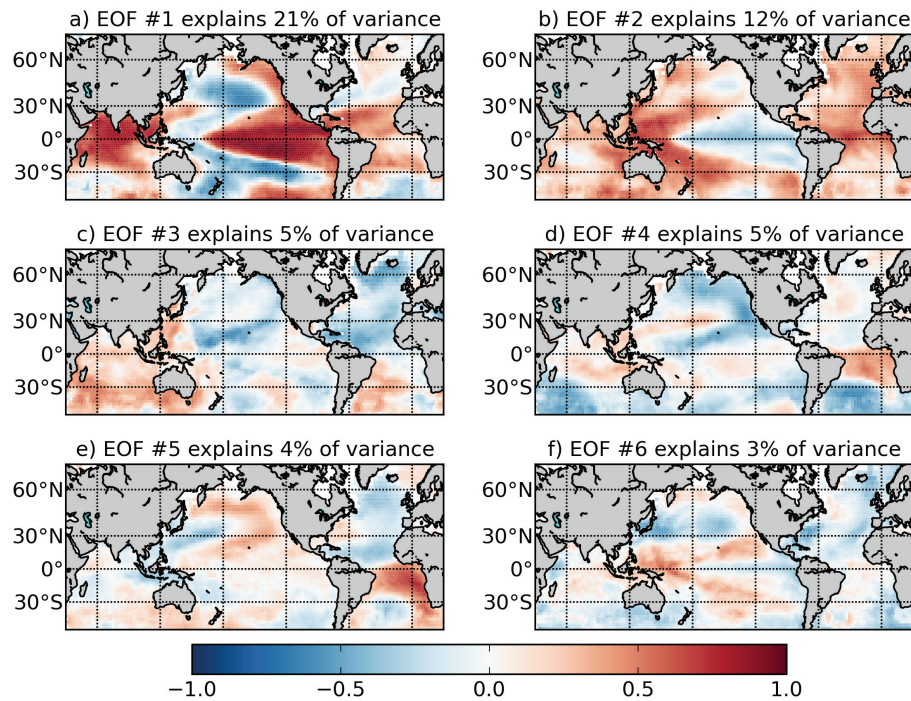


Fig. 4. First six EOFs determined for the same dataset as used to build the H-SST network.

Title Page

Abstract

Introduction

Conclusions

References

Tables

Figures

◀

▶

◀

▶

Back

Close

Full Screen / Esc

Printer-friendly Version

Interactive Discussion



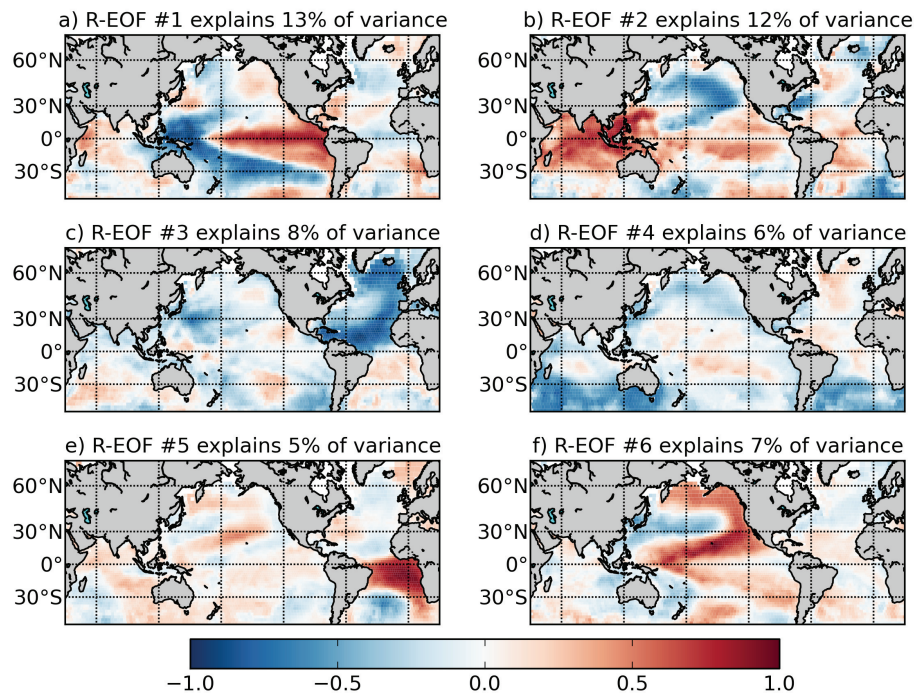
Network view of SST variabilityA. Tantet and
H. A. Dijkstra

Fig. 5. First six varimax-rotated EOFs estimated from the same dataset as used to build the H-SST network.

Title Page

Abstract

Introduction

Conclusions

References

Tables

Figures

◀

▶

◀

▶

Back

Close

Full Screen / Esc

Printer-friendly Version

Interactive Discussion



Network view of SST variability

A. Tantet and
H. A. Dijkstra

Title Page

Abstract

Introduction

Conclusions

References

Tables

Figures



Back

Close

Full Screen / Esc

Printer-friendly Version

Interactive Discussion

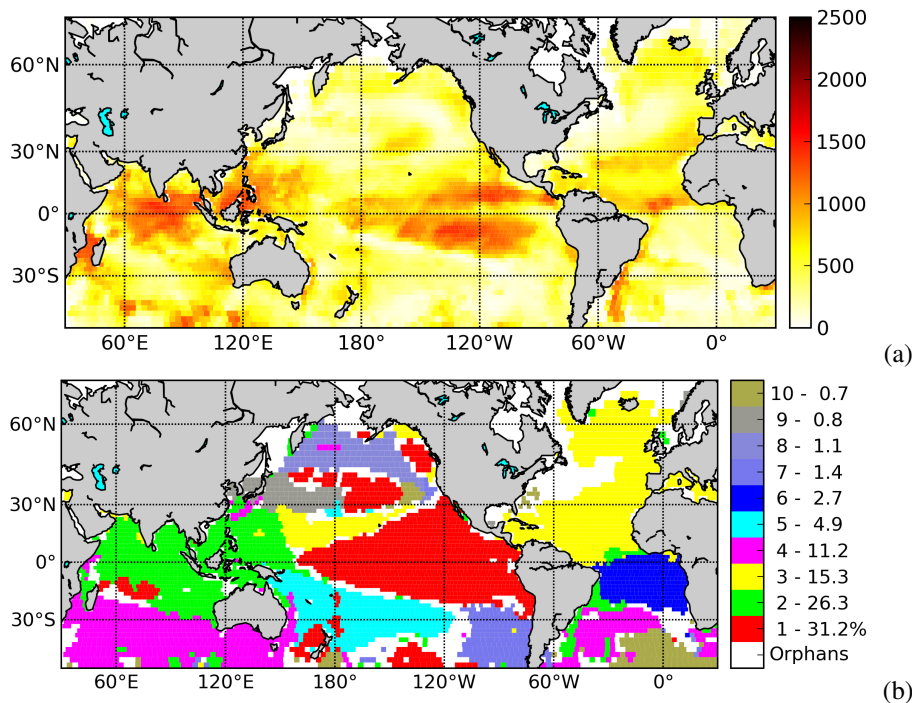


Fig. 6. (a) Degree centrality of the H-SST-LP8y network. The network was built using the same methodology as the H-SST network except that the time series were 8 yr low-pass filtered and a threshold $\tau = 0.6$ was used for significance; this results in an edge density $\rho = 0.087$. (b) Filtered communities in the H-SST-LP8y network.

Network view of SST variabilityA. Tantet and
H. A. Dijkstra

Title Page

Abstract

Introduction

Conclusions

References

Tables

Figures

◀

▶

◀

▶

Back

Close

Full Screen / Esc

Printer-friendly Version

Interactive Discussion

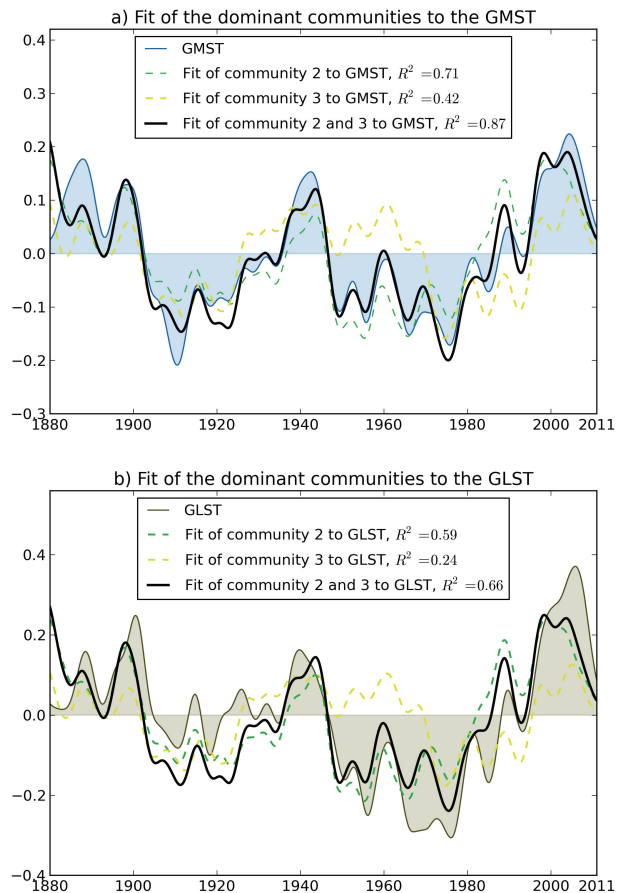


Fig. 7. Regression fits of the mean time series dominant communities of the H-SST-LP8y network to the (a) GMST and (b) GLST.

Network view of SST variability

A. Tantet and
H. A. Dijkstra

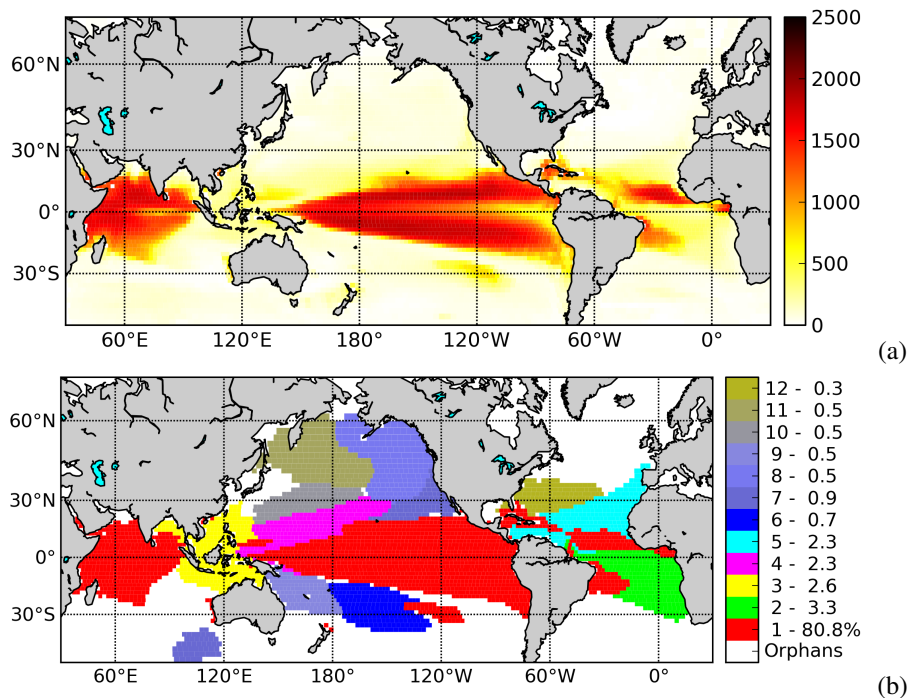


Fig. 8. (a) Degree centrality of the ESM-SST network. The network was built using the same methodology as for the H-SST network but using SST from the MPI-ESM-LR historical simulations. A threshold $\tau = 0.4$ was used as for the H-SST network leading to an edge density $\rho = 0.073$. (b) Filtered communities in the ESM-SST network.

Title Page

Abstract

Introduction

Conclusions

References

Tables

Figures

◀

▶

◀

▶

Back

Close

Full Screen / Esc

Printer-friendly Version

Interactive Discussion



Network view of SST variability

A. Tantet and
H. A. Dijkstra

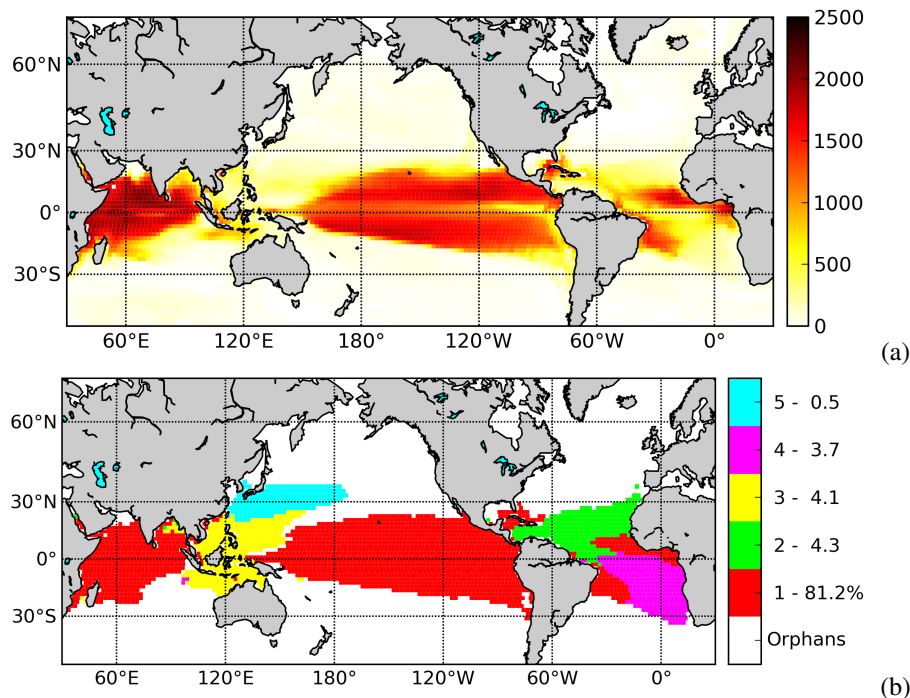


Fig. 9. (a) Degree centrality of the ESM-SST-LP8y network. The network was built using the same methodology as for the H-SST-LP8y network but using SST from the MPI-ESM-LR historical simulations. A threshold of $\tau = 0.6$ was used as for the H-SST network leading to an edge density $\rho = 0.077$. (b) Filtered communities in the ESM-SST-LP8y network.

Title Page

Abstract

Introduction

Conclusions

References

Tables

Figures

◀

▶

◀

▶

Back

Close

Full Screen / Esc

Printer-friendly Version

Interactive Discussion



Network view of SST variabilityA. Tantet and
H. A. Dijkstra

Title Page

Abstract

Introduction

Conclusions

References

Tables

Figures



Back

Close

Full Screen / Esc

Printer-friendly Version

Interactive Discussion

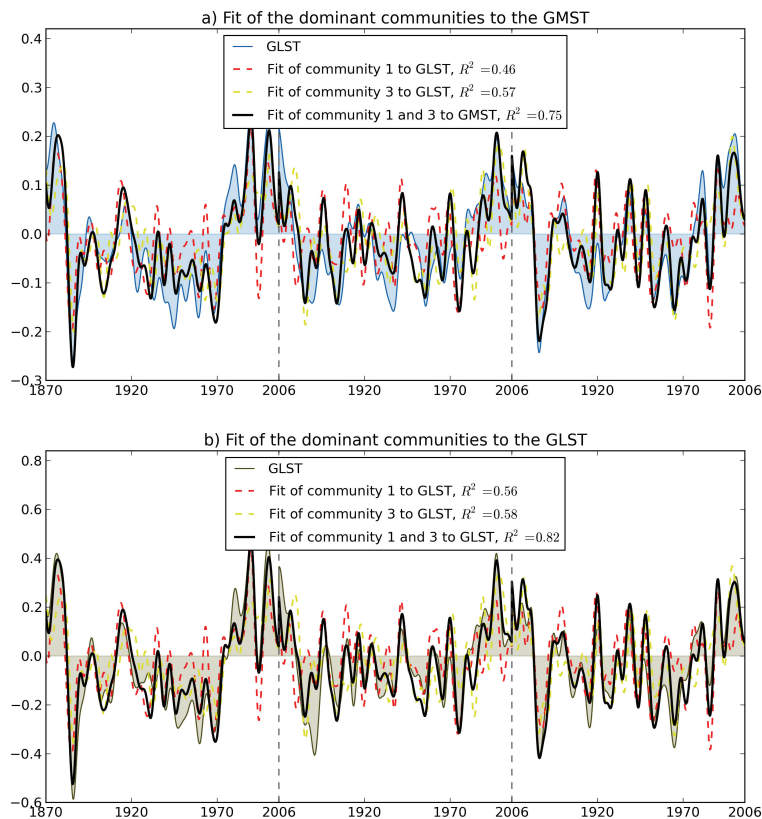


Fig. 10. Regression fits of the mean time series of the ESM-SST-LP8y dominant communities to the (a) GMST and (b) GLST.